Soft Matter

Accurate Estimation of the Polymer Coverage of Hairy Nanoparticles

Journal:	*Soft Matter*
Manuscript ID	SM-ART-06-2018-001311.R1
Article Type:	Paper
Date Submitted by the Author:	20-Aug-2018
Complete List of Authors:	Asai, Makoto; Columbia University in the City of New York, Chemical Engineering Zhao, Dan; Columbia University, Chemical Engineering Kumar, Sanat; Columbia University,

Accurate Estimation of the Polymer Coverage of Hairy Nanoparticles

Makoto Asai, Dan Zhao, Sanat K. Kumar*

Department of Chemical Engineering, Columbia University, New York, 10027, USA.

*Address correspondence to: sk2794@columbia.edu

ABSTRACT

Understanding and predicting the mechanisms underpinning the self-assembly of polymer-grafted nanoparticles (PGNPs) are important for controlling the engineering applications of these novel materials. The self-assembly of these materials is driven by their surfactancy, i.e., by the fact that the (inorganic) nanoparticles energetically dislike the (organic) polymer tethers. In previous work we developed a model in which a grafted polymer chain was treated as a rigid equivalent sphere (ES) which was impenetrable to the NPs, but completely penetrable to other ESs. This description, along with a geometric analogy with patchy particles, allowed us to facilely explain the self-assembly of PGNPs. However, since we model an ES as being completely penetrable to other ESs but impenetrable to the NPs the physical correspondence between a "real" grafted polymer and an ES is not clear. The application of the ES model to experiments and to computer simulations has therefore seen limited success, and only qualitative agreement has been obtained. In this paper, we develop a more realistic description, termed the modified ES (mES) model, based on the work of Daoud and Cotton on curved polymer brushes, which takes the impenetrability of the individual chain monomers into account. While this approach increases the complexity of our formalism, we find that the resulting mES model quantitatively captures computer simulation results on the structure of the PGNPs and also quantitatively explains their self-assembly over a broad range of conditions.

Introduction

A central challenge in improving the properties of polymer nanocomposites is to control the spatial dispersion of the nanoparticles (NPs).[1-4] One particularly facile approach is to graft the NPs with polymer chains.[5-8] It has been found that these grafted NPs behave akin to surfactants due to the dislike between the typically hydrophilic cores and the hydrophobic corona. This surfactant-like nature causes these tethered NPs to assemble into a large range of superstructures especially in the low grafting density, σ, limit (typically for $\sigma \lesssim 0.1$ chains/nm^2, see reference 9) , i.e., where the cores are not completely shielded from other cores by the corona.[9-23]

To understand this behavior, we have previously developed the equivalent sphere (ES) model.[24] A spherical NP of radius R_{n} randomly grafted with f chains was considered, where each chain was comprised of N catenated monomers. As a significant simplification we modeled each grafted polymer as a rigid ES of radius R. We further assumed that the ES served to exclude a "patch" on the grafting NP's surface where the core of another bare NP cannot contact. It is noted that the second NP has grafted polymers on its surface as well but for simplicity we only calculated the excluded area on the NP to another "bare" NP. This is reasonable in the low grafting density regime studied in the current paper, where the self-assembly of PGNPs most likely occurs. However, there was no excluded volume interactions between two (or more) ESs, either on a single NP or across multiple NPs. This last assumption is based on the fact that, while excluded volume interactions apply strictly at the level of two monomers, the centers of mass of two chains can overlap with only a small free energy cost.[25] The fraction (γ^*) of the NP surface that is excluded to a second bare NP due to an ES (or a single grafted chain) can then be derived:

$$\gamma^* = \frac{\alpha}{2(1+\alpha)} \tag{1}$$

Here, $\alpha \equiv R/R_{\mathrm{n}}$. When $\alpha \to \infty$, $\gamma^* \to 1/2$, which means that one ES can cover half of the surface of a NP in this limit. For f grafts the fraction (S^*) of the NP surface that is excluded to a second bare NP can then be described by analogy to random sequential adsorption:

$$\frac{dS^*}{df\gamma^*} = 1 - S^* \quad (0 \leq S^* \leq 1) \tag{2}$$

That is, we write that S^* can only increase if the newly grafted ES shields unexcluded parts of the surface. This yields $S^* = 1 - e^{-f\gamma^*}$, which we have found to be in good agreement with our simulation results on NPs literally grafted with ES. Thus, we have a means of describing the excluded surface area afforded by the grafted polymers on the surface of the NP with variations in f and α.

We then drew a geometric analogy between NPs grafted with ES and patchy particles. Regions on the NP surface from which a second NP is excluded (due to the presence of the ES) are defined as repulsive patches while the remaining NP surface is attractive to a second NP. In this representation, thus, the polymer chains (or the ESs) are abstracted away and only manifest themselves as an effective (angle and distance dependent) inter NP potential. With this mapping we can predict the self-assembled structures formed by a particular NP with knowledge of the S^* and the geometric structure of the PGNPs. Our idea, which has been previously discussed in reference 24, is sketched in Figure 1. When the polymer surface coverage S^* is large, we get well dispersed NPs. As the ES coverage decreases we first see the formation of small clumps comprised of 2-4 NPs. Further decreases in S^* yield linear strings of NPs and finally two and three-dimensional aggregates. Since this argument is purely geometrical, we can provide precise values of S^* where these "structural" transitions occur. We do not have the ability to decide if these are thermodynamic transitions or not.

In reference 24 we postulated that $R = \beta R_{\mathrm{g}}$ where R_{g} is the radius of gyration of the grafted polymer chain in a good solvent and β is an empirical fitting parameter. Figure 2 (a) uses the naive ansatz that $\beta = 1$ and we see that the ES model then only provides qualitative agreement with experimental data and simulation results from the literature.[24] For example, it is clear that regions where strings are formed in

the Monte Carlo simulations are predicted to form clumps etc. Clearly, there is room for improvement in terms of this model prediction.

Instead, we have empirically found that we need to use $\beta \approx 0.46$ to get better agreement with experiments and simulations.[24, 26] However, it is unclear why we have to use an R that is less than R_g and whether the factor $\beta = 0.46$ is universal. When this information is absent, the conventional ES model is limited in terms of structure prediction. Additionally, the model has a major simplification in that the excluded volume interactions between two (or more) grafted chains are ignored since the ES are assumed to be fully penetrable to each other but completely impenetrable to the core of another NP. We conjecture that dispensing with these assumptions, by modeling the grafts more realistically, should allow for a more reliable representation for these systems.[27] So, in this paper, we introduce this improvement to the conventional ES model. In particular, we use the Daoud-Cotton model for polymer brushes to more accurately model the polymer chains in this situation. By validating against computer simulations, we show that this model provides an improved description of the structure of these NPs and hence their self-assembly behavior. Thus, we propose that this modified ES (mES) model can be used to reliably understand the self-assembly of this class of materials.

Results and Discussion

mES Model

The basic strategy for constructing the mES model is to more accurately account for the structural properties of real polymer brush chains than in the ES model, i.e., to account for the excluded volume interactions at the level of two monomers. According to the Daoud–Cotton picture of a star polymer,[28] which can be extended to describe polymer statistics on curved surfaces,[29] the grafting process only weakly changes the effective chain size, R, i.e., by a factor $f^{-1/5}$, where f is the number of grafts. Since R should be a function of N (the degree of polymerization for the grafted chain) and f, we assume that an

appropriate size of the brush chain follows $R(N,f) = R(N) \times R(f)$, that is we assume that the N and f dependences are separable.

Before considering the f dependency, first, we investigate the statistics of a single grafted polymer ($f = 1$). Let us consider one free (ungrafted) polymer chain with radius of gyration R_{g} and polymerization degree N. The monomer density at a distance r from the polymer's center of mass is [30]

$$\rho(r) = \frac{ND}{4\pi R_{\mathrm{g}}^{D}} r^{D-3} \tag{3}$$

Here D is the fractal dimension of the chain, and we use the mass balance condition $\int_0^{2\pi} d\varphi \int_0^{\pi} \sin\theta \, d\theta \int_0^{R_{\mathrm{g}}} r^2 \rho(r) dr = N$. If the chain were fully collapsed then $D = 3$ and Eq. (3) suggests that the monomer density profile is constant, as expected. For a Gaussian chain $D = 2$ and so the monomer density decreases with increasing r. We assume that a single grafted chain on the NP (NP1) surface has the same density distribution about the center of mass as the ungrafted analog and calculate the number $\Psi\left(L, R_{\mathrm{n}}, R_{\mathrm{g}}\right)$ of monomer units of the polymer overlapping with a second bare NP (NP2) of radius R_{n} which is placed at a distance L from the center of mass of the polymer chain (see Appendix Figure A1). That is, we take a NP1 with a grafted chain and ask as to how much grafted chain-NP2 overlap this system has when a NP2 is brought to a distance L from the grafted polymer chain's center of mass. To calculate this quantity, the following volume integration should be performed on the region where the NP2 and the polymer grafted on the NP1 overlap.

$$\Psi\left(L, R_{\mathrm{n}}, R_{\mathrm{g}}\right) = \int \rho(r) dV \tag{4}$$

While the calculation of this integration is straightforward, it is mathematically tedious and deferred to Appendix A. However, illustrative numerical examples of the behavior of this function are shown in Figure 3. We assumed $2R_{\mathrm{g}} = N^{1/D}$ and $D = 5/3$, which describes the radius of gyration of coarse-grained Kremer-Grest chains in good solvent.[31] Some general comments are in order. In general, the overlap function $\Psi\left(L, R_{\mathrm{n}}, R_{\mathrm{g}}\right)$ increases with decreasing L, till it reaches a plateau value at small L. Note that $\Psi\left(R_{\mathrm{n}} + R_{\mathrm{g}}, R_{\mathrm{n}}, R_{\mathrm{g}}\right) = 0$ in the situation where the distance between the NP2 and the center of mass

of the grafted polymer chain is $L = R_{\mathrm{n}} + R_{\mathrm{g}}$ or for any larger separations since there is no overlap. In addition, when $R_{\mathrm{g}} \leq R_{\mathrm{n}}$, the chain is completely inside NP2 when $L = 0$ and thus $\Psi(0, R_{\mathrm{n}}, R_{\mathrm{g}}) = N$. On the other hand, when $R_{\mathrm{g}} > R_{\mathrm{n}}$, the maximum value in Ψ is less than N, because the chain is not completely inside the NP2 even when their centers of mass coincide: thus, the NP2 can only overlap with a part of the polymer chain.

While the discussion above focuses on the overlap between a polymer chain grafted onto a NP1 and the core of a NP2, the more important quantity is what fraction of the NP1 surface is inaccessible to NP2 due to the presence of the grafted chain. To make this calculation we place NP2 in contact with the surface of NP1 and calculate the number Ψ of monomer units of the polymer overlapping with NP2 (see Figure 4(a)). The distance between the center of mass of the polymer chain and NP2 is L. When $\Psi \geq 1$ then this point corresponds to an overlap between NP2 and the graft – this point is thus excluded to NP2. We now place the NP1 on several points on the surface: The ratio of the number of points with $\Psi \geq 1$ to the total number sampled should be the exclusion area γ^* for a polymer chain for NP2. Therefore, we define γ^* as follows:

$$\gamma^* = \frac{1}{4\pi}\int_0^{2\pi} d\varphi \int_0^{\pi} \bar{\Psi} \cdot \sin\theta \, d\theta \tag{5}$$

$$\bar{\Psi} \equiv \begin{cases} 1, & \Psi \geq 1 \\ 0, & \Psi < 1 \end{cases} \tag{6}$$

Then, we can determine R using Eq. (1). The geometric concept is shown in Figure 4(b). We evaluated Eq. (5) numerically since it is difficult to analytically calculate it (Figure 5(a)-(c)). As a reference, we also show γ^* calculated by the ES model. In this case, we used Eq. (1) with $\beta = 1(R = R_{\mathrm{g}})$. This figure critically illustrates the qualitative errors in our previous ES model. In the ES model, γ^* monotonically increases with increasing N and eventually reaches the theoretical maximum value $(= 1/2)$. This result simply follows from the fact that there is strict impenetrability between an ES and the core of a NP2. On the other hand, in the mES model, γ^* starts to decrease when N becomes sufficiently large. This is because, when $R_{\mathrm{n}} \ll R_{\mathrm{g}}$, the NP2 cannot overlap with the whole polymer chain. To illustrate this point,

we consider the case when NP1, NP2 and the polymer are collinear, but with NP1 and NP2 being in contact. Under these conditions, $L = R_{\mathrm{g}} - R_{\mathrm{n}} \gg 0$. Therefore, the center of NP2 will only experience the very low-density perimeter of the polymer coil. This means that, in the long chain limit, the NP2 and the polymer chain interact minimally leading to small γ^* values.

Moreover, we estimated R corresponding to these γ^* using Eq. (1) (Figure 5 (d)). In the conventional ES model, since R was assumed to be related linearly to R_{g}, R depends on only N ($R \propto R_{\mathrm{g}} \propto N^{1/D}$). However, in the mES model we find that R depends, not only on N, but also on R_{n}. Furthermore, in the large limit of large N, R approaches zero, which corresponds to γ^* approaching zero. From the above discussion, it is clear that the initial assumption built into the ES model that R is simply proportional to R_{g}, $R = \beta R_{\mathrm{g}}$, is incorrect.

To prove the validity of the mES model, we performed coarse-grained Molecular Dynamics simulations using the Kremer-Grest model.[31] We directly measured the excluded area provided by one grafted chain, γ^*, to the core of a NP2 in the range of $5 \leq N \leq 10^4$ for up to 10^7-10^8 MD time steps, long enough to achieve equilibrium in all cases. We set $R_{\mathrm{n}} = 7.0$. Simulation details are described in the Methods Section. First, we calculate the N-dependence of the R_{g} of one grafted polymer chain. We obtained $R_{\mathrm{g}} = 0.33N^{0.70} (N \leq 50)$ and $R_{\mathrm{g}} = 0.49N^{0.60} (N > 50)$. Next, we directly measured γ^* in the simulations by tessellating the surface of the NP1 using 4112 points placed at the vertices of a spherical crystal following the symmetry of a (20, 20) icosadeltahedron. We fixed the center of NP1 and performed MD simulations of a single tethered polymer. For each MD snapshot, we assign $p_i = 1$ if there are polymer beads which overlap with a NP2 located on the i^{th} point ($i = 1, 2, \ldots, 4112$) of the surface of NP1, otherwise $p_i = 0$. By taking the time-average $\langle p_i \rangle_t$ of p_i, we calculate the excluded area ratio as $\gamma^* = \sum_i^{4112} \langle p_i \rangle_t / 4112$.

Figure 6(a) shows an example of the surface distribution of $\langle p_i \rangle_t$. We see that there is a spherical cap-shaped excluded area formed by a grafted chain on the surface of NP1, indicating that the geometric concept expressed by Eq. (1), commonly used in the ES and mES models, is reasonable. However,

because a polymer is treated as a rigid sphere in the original ES model, $\langle p_i \rangle_t$ should be 1 within the spherical cap-shaped excluded area. In fact, $\langle p_i \rangle_t$ varies gradually as shown in Figure 6(a). Figure 6(b) shows the N-dependence of γ^*. In the ES model, we calculated γ^* using Eq. (1) assuming $\beta = 1\left(R = R_{\mathrm{g}}\right)$. On the other hand, in the mES model, we calculated γ^* using Eq. (5) without any assumptions. As a result, the ES model overestimates γ^* compared to those measured in simulations, especially as N becomes larger. On the other hand, we found that γ^*calculated in the mES model was in good agreement with those measured in simulations over the whole range of N, including the non-monotonic dependence of γ^* on N observed in simulations. Furthermore, we converted γ^* to an effective R, the size of an ES, using Eq. (1) as shown in Figure 6(c). The size of an ES thus does not monotonically depend on the R_{g} of the chain. We thus have a full understanding of the surface coverage afforded by a single grafted chain.

Next, we account for the effect of multiple grafted chains by assuming the validity of the Daoud-Cotton ansatz.[28] Note that the separation of the N and f dependence inherent in our approach is only reasonable when the grafting density is relatively low, i.e., when the chains are not significantly distorted. We thus estimate the f-dependence of $R(f)$ as follows.

$$R = R(N, R_{\mathrm{n}}) \cdot f^{-1/5} \tag{7}$$

To confirm the validity of Eq. (7), we calculated the f-dependence of γ^* of a polymer chain in the range $1 \leq f \leq 100$ and $N = 5, 100, 200$ using MD simulations. The images in Figure 7(a) show examples of the surface distribution of $\langle p_i \rangle_t$. We found that as f becomes larger, the distribution of $\langle p_i \rangle_t$ becomes narrower. (Note that this is a plot of the probability density associated with one representative chain out of the f that are grafted to the NP1 surface: as f increases the distribution of a single chain narrows in space as may be expected.) We converted these γ^* to R using Eq. (1). Figures 7(a) and 7(b) show the f-dependence of γ^* and R as determined from the simulations, respectively. We confirm the scaling law: $R \propto f^{-1/5}$ in the large N (≥ 200) / relatively large f (> 20) limit. On the other hand, the scaling law does not work for smaller N and f. According to Daoud-Cotton theory, polymers are not influenced by

the curvature of the NP surface when the end-to-end distance of the chains $R_e \ll R_n$. Indeed, we find that $R_e \approx 4.2R_n$ for $N = 200$, $R_e \approx 2.8R_n$ for $N = 100$, and $R_e \approx 1.8R_n$ for $N = 50$, respectively, suggesting that we are approaching the limits of this theory for small N.

We directly measured the total excluded area ratio S^* in the simulations with f grafted chains – this corresponds to the fraction of the NP1 surface that is inaccessible to the NP2 due to the presence of the grafted chains. In addition, we compared S^* with those predicted by the ES and mES models. In the ES and mES models, we first calculated R using the hypothetical relationship, $R = \beta R_g$ and Eq. (7), respectively. Note that since Eq. (7) does not work in the region of small f and small N as discussed in Figure 7, we used the fitted functions obtained from Figure 7(b) as follows: For $N = 50$, $R = 3.45f^{-0.046}$ $(f < 30)$. For $N = 100$, $R = 4.39f^{-0.128}$ $(f < 20)$. By substituting R into Eq. (1), we calculated γ^*. Finally, using Eq. (2), we calculated S^* as shown in Figure 8(a)-(c). The mES model shows good agreement with simulation values of S^*, and the difference between the ES and mES models becomes larger with increasing N. This is due to the fact that the difference of R between the ES and mES models is small until $N \approx 50$ (see Figure 6(c)).

Self-Assembly

Finally, we examine whether the mES model can quantitatively explain experimental results and simulation findings for the self-assembly of this class of PGNPs. To this end, we use the information on experimental conditions (N, f, R_n) and calculate the effective R for each condition using the mES model and Eq. (1). Then, using the geometric analogy with patchy particles,[24] discussed above in the context of Figure 1, we predicted the self-assembled structures formed and compared them with the morphologies reported. We refer to the following different systems: I) polystyrene-grafted silica NPs in a polystyrene matrix (PS-g-silica NPs)[10, 32], II) mixed bimodal polystyrene-poly(2-vinylpyridine) brush coated silica NPs in a polystyrene matrix (PS-P2VP-g-silica NPs)[32], III) polystyrene-b-poly(2-vinylpyridine) block copolymer physically absorbed silica NPs in a polystyrene matrix (PS-b-P2VP-a-silica NPs)[33], IV)

Coarse-grained bead-spring polymer-grafted onto NPs studied by Monte Carlo simulation (CG simulation)[10]. In the case of experiments using polystyrene, we estimated R_g as $R_g \approx a(N/6)^{1/2}$, which is the unperturbed radius of gyration in the melt and a is the segment length of a polystyrene chain, which was estimated to be 5 Å.[34] In case III), we assumed that since P2VP adsorbs completely on the surface of NP, R_g of BCP is calculated by only taking the PS block into account. We show all necessary parameters in Tables 1(a) and 1(b). With given R_n, N and f we estimate R by Eq. (7), and then calculate α as $\alpha \equiv R/R_n$. Figure 2b shows each sample plotted on the $\alpha - f$ plane of the theoretical phase diagram of the self-assembly of PGNPs. We find that self-assembled structures found in simulations of coarse grained models and also three different classes of experiments are in good agreement with the mES - based theoretical predictions over a broad range of α and f values. We therefore believe that the mES model allows us to capture the self-assembly behavior of these PGNPs without the use of any adjustable parameters.

Conclusions

We propose a new calculation method for the surface coverage afforded by polymer chains grafted on to spherical NP surfaces. This calculation method can accurately predict the area of the NP surface that is excluded to another NP by the presence of the grafted chain. A simple extension of this model by adopting ideas from the Daoud-Cotton approach allows us to model NPs with multiple grafts. All of these results are in quantitative agreement with coarse grained simulations. Further, we draw an analogy of these grafted particles to patchy NPs, and from there predict the self-assembled structures that are formed. These results, which therefore have no adjustable parameters, are in excellent agreement with appropriately curated previous experiments and simulations. We therefore propose that the mES model can apparently be used to quantitatively understand the structure and the anisotropic self-assembly of this class of polymer grafted nanoparticles. Importantly, although in the current paper we only focus on the

case of good solvent conditions, our model can be naturally extended to other solvent qualities (*e.g.* theta solvent or poor solvent) by reformulating the Daoud-Cotton model and the associated scaling laws.

Methods

Simulation Model

Grafted polymers are represented using the coarse-grained bead-spring model of Kremer and Grest.[31] Each chain contains N beads of mass $m = 1$. All beads interact via the Lennard-Jones (LJ) potential.

$$U_{\mathrm{p}}(r) = \begin{cases} 4\epsilon\left[\left(\frac{\sigma}{r}\right)^{12} - \left(\frac{\sigma}{r}\right)^{6}\right], & r \le r_{\mathrm{c}} \\ 0, & r > r_{\mathrm{c}} \end{cases} \quad (9)$$

where r is the distance between two beads, ϵ is the Lennard-Jones unit of energy, and σ is the bead diameter. We set $r_{\mathrm{c}} = 2^{1/6}\sigma$. Beads along the chain are connected by an additional unbreakable finitely extensible nonlinear elastic (FENE) potential $U_{\mathrm{FENE}}(r) = -1/2\, k{l_{\mathrm{max}}}^2 \ln[1 - (r/l_{\mathrm{max}})^2]$, with $l_{\mathrm{max}} = 1.5\sigma$ and $k = 30\epsilon/\sigma^2$. We use the expanded LJ potential for pair interactions between colloid-colloid and colloid-polymer beads as follows;

$$U(r) = \begin{cases} 4\epsilon\left[\left(\frac{\sigma}{r-\Delta}\right)^{12} - \left(\frac{\sigma}{r-\Delta}\right)^{6}\right], & r \le r_{\mathrm{c}} + \Delta \\ 0, & r > r_{\mathrm{c}} + \Delta \end{cases} \quad (10)$$

Here, we choose $\Delta = 4\sigma$ and $\Delta = 2\sigma$ for colloid-colloid and colloid-polymer bead interactions, respectively. One end bead of the grafted polymer is fixed on the surface of the colloid (grafting point). f grafting points are randomly located on the surface. $N_{\mathrm{NP}}(= 4^3)$ colloids have different patterns of grafting points arrangements.

Molecular Dynamics Simulation

All simulations are carried out using the LAMMPS parallel MD package. NVT MD simulations are performed in an orthogonal cubic simulation box. Temperature T is set to $1.0\,\epsilon/k_{\mathrm{B}}$and is maintained by a Langevin thermostat with a damping constant $\Gamma = 0.01\sigma^{-1}(m/\epsilon)^{-1/2}$. k_{B} is Boltzmann's constant. The

NPs' positions are fixed and only the dynamics of grafted polymers is enumerated. The simulations are run for $10^6 - 10^8$ time steps of length $dt = 0.005\sqrt{m\sigma^2/\epsilon}$ to equilibrate the system and then another $10^7 - 10^8$ time steps for each observation.

Appendix

We will explain the derivation of Ψ, which depends on R_g, R_n and L. Figure A1(a)-(e) show 5 different geometric situations to consider. Here a polymer chain grafted on the surface of a NP1 is drawn as a spherical sphere with radius of R_g (hereinafter called "a polymer coil") and it has fractal structure inside the sphere. The integration range is the overlapping range of two spheres (the polymer coil and the NP2), and the coordinates within the integration range are denoted by (r, θ, φ). θ_m, r_{max} and r_{min} are the maximum angle and the maximum and the minimum length in the integration range of θ and r, respectively.

(I) $\boldsymbol{R_g \leq R_n}$

In this case, we have to consider the following three situations for the range of L:

$\boldsymbol{0 \leq L \leq R_n - R_g}$: the polymer coil is completely inside the NP2. As an example, Figure A1(a) shows a case where $L = R_n - R_g$. In this case, Eq. (4) becomes:

$$\boldsymbol{\Psi(L, R_n, R_g) = \frac{ND}{4\pi R_g^D} \int_0^{2\pi} d\varphi \int_0^{\pi} \sin\theta \, d\theta \int_0^{R_g} r^{D-1} dr} \quad \text{(A1)}$$

As a result, we derive:

$$\boldsymbol{\Psi = N} \quad \text{(A2)}$$

$\boldsymbol{R_n - R_g \leq L \leq R_n}$: the polymer coil and the NP2 are partially overlapping and the center of the polymer coil (O_p) is inside the NP2 (O_n) and vice versa. As an example, Figure A1 (b) shows a case where $L = R_n$. In this case, Eq. (4) becomes:

$$\boldsymbol{\Psi\left(L, R_{\mathrm{n}}, R_{\mathrm{g}}\right) = \frac{ND}{4\pi R_{\mathrm{g}}^{D}}\left\{\int_{0}^{2\pi} d\varphi \int_{0}^{\theta_{\mathrm{m1}}} \sin\theta\, d\theta \int_{0}^{R_{\mathrm{g}}} r^{D-1} dr + \int_{0}^{2\pi} d\varphi \int_{\theta_{\mathrm{m1}}}^{\pi} \sin\theta\, d\theta \int_{0}^{r_{\max}} r^{D-1} dr\right\}} \quad \text{(A3)}$$

Here, the integration range should be divided into two, corresponding to the first and second term of the right side, respectively. The first and second integration range are represented by filled and dotted areas, respectively in figure A1 (b). Here, θ_{m1} is the maximum angle of integration range of θ in the first term of right side. So $\cos\theta_{\mathrm{m1}} = (L^2 + R_{\mathrm{g}}^2 - R_{\mathrm{n}}^2)/2R_{\mathrm{g}}L$ and $r_{\max} = L\cos\theta - \sqrt{(L\cos\theta)^2 - (L^2 - R_{\mathrm{n}}^2)}$. As a result, we obtain:

$$\boldsymbol{\Psi = \frac{N}{2}\left\{1 - \frac{\left(L^2 + R_{\mathrm{g}}^2 - R_{\mathrm{n}}^2\right)}{2R_{\mathrm{g}}L}\right\} + \frac{N}{4R_{\mathrm{g}}^{D}L(D^2-1)}\left[R_{\mathrm{g}}^{D-1}\left\{(D+1)\left(R_{\mathrm{n}}^2 - L^2\right) + (D-1)R_{\mathrm{g}}^2\right\} - 2(R_{\mathrm{n}} - L)^{D}(DR_{\mathrm{n}} + L)\right]} \quad \text{(A4)}$$

$\boldsymbol{R_{\mathrm{n}} \le L \le R_{\mathrm{n}} + R_{\mathrm{g}}}$**:** the polymer coil and the NP2 are partially overlapping and the center of the polymer coil (O_p) is outside the NP2 and vice versa (Figure A1(c)). In this case, Eq. (4) becomes:

$$\Psi\left(L, R_{\mathrm{n}}, R_{\mathrm{g}}\right) = \frac{ND}{4\pi R_{\mathrm{g}}^{D}} \int_{0}^{2\pi} d\varphi \int_{0}^{\theta_{\mathrm{m}}} \sin\theta\, d\theta \int_{r_{\min}}^{R_{\mathrm{g}}} r^{D-1} dr \quad \text{(A5)}$$

Here $\cos\theta_{\mathrm{m}} = (L^2 + R_{\mathrm{g}}^2 - R_{\mathrm{n}}^2)/2R_{\mathrm{g}}L$ and $r_{\min} = L\cos\theta - \sqrt{(L\cos\theta)^2 - (L^2 - R_{\mathrm{n}}^2)}$. As a result, we can derive:

$$\Psi = \frac{N}{2}\left[1 - \frac{\left(L^2 + R_{\mathrm{g}}^2 - R_{\mathrm{n}}^2\right)D^2}{2R_{\mathrm{g}}L(D^2-1)} + \left(\frac{L - R_{\mathrm{n}}}{R_{\mathrm{g}}}\right)^{D}\left\{\frac{DR_{\mathrm{n}} + L}{(D^2-1)L}\right\} - \frac{\left(L^2 - R_{\mathrm{g}}^2 - R_{\mathrm{n}}^2\right)D}{2R_{\mathrm{g}}L(D^2-1)}\right] \quad \text{(A6)}$$

(II) $\boldsymbol{R_{\mathrm{n}} \le R_{\mathrm{g}} \le 2R_{\mathrm{n}}}$

$\mathbf{0 \le L \le R_g - R_n}$**:** the NP2 is completely inside the polymer coil and the center of the polymer coil (O_p) is inside the NP2. As an example, Figure A1 (d) shows a case where $L = R_n - R_g$. In this case, Eq. (4) can be described as:

$$\Psi(L, R_n, R_g) = \frac{ND}{4\pi R_g^D} \int_0^{2\pi} d\varphi \int_0^{\pi} \sin\theta \, d\theta \int_0^{r_{max}} r^{D-1} dr \quad \text{(A7)}$$

Here, $r_{max} = L\cos\theta + \sqrt{(L\cos\theta)^2 - (L^2 - R_n^2)}$. As a result, we derived:

$$\boldsymbol{\Psi = \frac{N}{2R_g^D L(D^2 - 1)} \{(R_n + L)^D (DR_n - L) - (R_n - L)^D (DR_n + L)\}} \quad \text{(A8)}$$

$\mathbf{R_g - R_n \le L \le R_n}$**:** the polymer coil and the NP2 are partially overlapping and the center of the polymer coil (O_p) is inside the NP2 (O_n) and vice versa. This case is geometrically same with a case of Figure A1 (b), but just different of relative size of R_g and R_n. The obtained result is equal to Eq. (A4).

$\mathbf{R_n \le L \le R_n + R_g}$**:** the polymer coil and the NP2 are partially overlapping and the center of the polymer coil (O_p) is outside the NP2 and vice versa (Figure A1(c)). This case is geometrically same with a case of Figure A1 (c), but just relative size of R_g and R_n. The obtained result is equal to Eq. (A6).

(III) $\mathbf{2R_n \le R_g}$

$\mathbf{0 \le L \le R_n}$**:** the NP2 is completely inside the polymer coil and the center of the polymer coil (O_p) is inside the NP2. This case is geometrically same with a case of Figure A1 (d), just different of relative size of R_g and R_n. The obtained result is equal to Eq. (A8).

$\mathbf{R_n \le L \le R_g - R_n}$**:** the NP2 is completely inside the polymer coil and the center of the polymer coil (O_p) is outside the NP2. As an example, Figure A1 (e) shows a case where $L = R_g - R_n$. In this case, Eq. (4) becomes:

$$\Psi(L, R_{\mathrm{n}}, R_{\mathrm{g}}) = \frac{ND}{4\pi R_{\mathrm{g}}^{D}} \int_0^{2\pi} d\varphi \int_0^{\theta_{\mathrm{m}}} \sin\theta \, d\theta \int_{r_{\min}}^{r_{\max}} r^{D-1} dr \qquad \text{(A9)}$$

Here $\sin\theta_{\mathrm{m}} = R_{\mathrm{n}}/L$, $r_{\max} = L\cos\theta + \sqrt{(L\cos\theta)^2 - (L^2 - R_{\mathrm{n}}^2)}$, and $r_{\min} = L\cos\theta - \sqrt{(L\cos\theta)^2 - (L^2 - R_{\mathrm{n}}^2)}$. As a result, we can derive:

$$\boldsymbol{\Psi = \frac{N}{2R_{\mathrm{g}}^{D} L(D^2 - 1)} \{(L - R_{\mathrm{n}})^{D}(DR_{\mathrm{n}} + L) + (L + R_{\mathrm{n}})^{D}(DR_{\mathrm{n}} - L)\}} \qquad \text{(A10)}$$

$R_{\mathrm{g}} - R_{\mathrm{n}} \le L \le R_{\mathrm{n}} + R_{\mathrm{g}}$: the polymer coil and the NP2 are partially overlapping and the center of the polymer coil (O_p) is outside the NP2 and vice versa. This case is geometrically same with a case of Figure A1 (c), just different of relative size of R_{g} and R_{n}. The obtained result is equal to Eq. (A6).

Acknowledgements

The authors thank the National Science Foundation for financial support of this work. S.K.K. acknowledges the National Science Foundation through grant DMR-1507030.

Competing financial interests: The authors declare no competing financial interests.

References

1. R. Krishnamoorti and R. A. Vaia, *Journal of Polymer Science Part B: Polymer Physics*, 2007, **45**, 3252-3256.
2. M. E. Mackay, A. Tuteja, P. M. Duxbury, C. J. Hawker, B. Van Horn, Z. Guan, G. Chen and R. Krishnan, *Science*, 2006, **311**, 1740-1743.
3. R. Krishnamoorti, *MRS bulletin*, 2007, **32**, 341-347.
4. A. Bansal, H. Yang, C. Li, K. Cho, B. C. Benicewicz, S. K. Kumar and L. S. Schadler, *Nature materials*, 2005, **4**, 693-698.

5. D. L. Green and J. Mewis, *Langmuir*, 2006, **22**, 9546-9553.

6. A. Bansal, H. Yang, C. Li, B. C. Benicewicz, S. K. Kumar and L. S. Schadler, *Journal of Polymer Science Part B: Polymer Physics*, 2006, **44**, 2944-2950.

7. C.-K. Wu, K. L. Hultman, S. O'Brien and J. T. Koberstein, *Journal of the American Chemical Society*, 2008, **130**, 3516-3520.

8. S. E. Harton and S. K. Kumar, *Journal of Polymer Science Part B: Polymer Physics*, 2008, **46**, 351-358.

9. S. K. Kumar, N. Jouault, B. Benicewicz and T. Neely, *Macromolecules*, 2013, **46**, 3199-3214.

10. P. Akcora, H. Liu, S. K. Kumar, J. Moll, Y. Li, B. C. Benicewicz, L. S. Schadler, D. Acehan, A. Z. Panagiotopoulos, V. Pryamitsyn, V. Ganesan, J. Ilavsky, P. Thiyagarajan, R. H. Colby and J. F. Douglas, *Nature Materials*, 2009, **8**, 354-U121.

11. M. Belkin, A. Snezhko, I. Aranson and W.-K. Kwok, *Physical Review Letters*, 2007, **99**, 158301.

12. M. Seul and D. Andelman, *Science*, 1995, **267**, 476.

13. Z. Tang, Z. Zhang, Y. Wang, S. C. Glotzer and N. A. Kotov, *Science*, 2006, **314**, 274-278.

14. K. Van Workum and J. F. Douglas, *Physical Review E*, 2006, **73**, 031502.

15. S. N. Fejer and D. J. Wales, *Physical review letters*, 2007, **99**, 086106.

16. E. Rabani, D. R. Reichman, P. L. Geissler and L. E. Brus, *Nature*, 2003, **426**, 271-274.

17. S. Gupta, Q. Zhang, T. Emrick, A. C. Balazs and T. P. Russell, *Nature Materials*, 2006, **5**, 229-233.

18. J. Oberdisse, *Soft matter*, 2006, **2**, 29-36.

19. M. Li, H. Schnablegger and S. Mann, *Nature*, 1999, **402**, 393-395.

20. A. K. Boal, F. Ilhan, J. E. DeRouchey, T. Thurn-Albrecht, T. P. Russell and V. M. Rotello, *Nature*, 2000, **404**, 746-748.

21. C. Pacholski, A. Kornowski and H. Weller, *Angewandte Chemie International Edition*, 2002, **41**, 1188-1191.

22. J. Kao, K. Thorkelsson, P. Bai, B. J. Rancatore and T. Xu, *Chemical Society Reviews*, 2013, **42**, 2654-2678.

23. B. Gao, G. Arya and A. R. Tao, *Nature nanotechnology*, 2012, **7**, 433-437.

24. M. Asai, A. Cacciuto and S. K. Kumar, *Soft Matter*, 2015, **11**, 793-797.

25. A. A. Louis, P. G. Bolhuis, J. P. Hansen and E. J. Meijer, *Phys Rev Lett*, 2000, **85**, 2522-2525.

26. N. Bachhar, Y. Jiao, M. Asai, P. Akcora, R. Bandyopadhyaya and S. K. Kumar, *Macromolecules*, 2017, **50**, 7730-7738.

27. M. Asai, D. Zhao and S. K. Kumar, *ACS Nano*, 2017, **11**, 7028-7035.

28. M. Daoud and J. Cotton, *Journal de Physique*, 1982, **43**, 531-538.

29. K. Ohno, T. Morinaga, S. Takeno, Y. Tsujii and T. Fukuda, *Macromolecules*, 2007, **40**, 9143-9150.

30. P.-G. De Gennes and T. A. Witten, AIP, 1980.

31. K. Kremer and G. S. Grest, *The Journal of Chemical Physics*, 1990, **92**, 5057-5086.

32. D. Zhao, M. Di Nicola, M. M. Khani, J. Jestin, B. C. Benicewicz and S. K. Kumar, *ACS Macro Letters*, 2016, **5**, 790-795.

33. D. Zhao, M. Di Nicola, M. M. Khani, J. Jestin, B. C. Benicewicz and S. K. Kumar, *Soft Matter*, 2016, **12**, 7241-7247.

34. J. Brandrup, E. H. Immergut, E. A. Grulke, A. Abe and D. R. Bloch, *Polymer handbook*, Wiley New York etc, 1989.

Figures

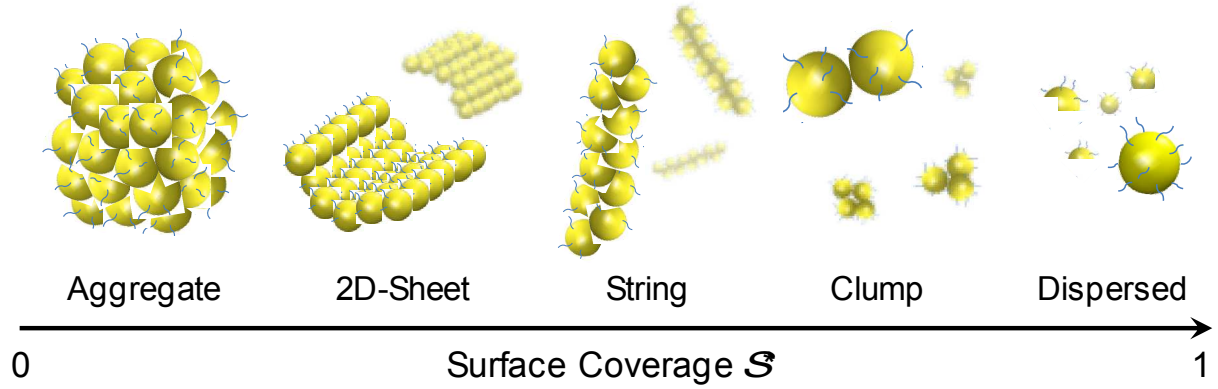

Figure 1: Different aggregate morphologies with increasing polymer surface coverage, following Asai *et al*. [Ref. 24] (Aggregate) three-dimensional and (2D-Sheet) two-dimensional aggregates (coordination number ≥ 4); (String) one dimensional linear aggregate (coordination number = 2 ~ 3); (Clump) small aggregates including dimers, trimers and tetramers (coordination number = 1 ~ 3); (Dispersed) isolated particles with full surface coverage (coordination number = 0). The formula for S^* for each morphology is presented in Ref. 24.

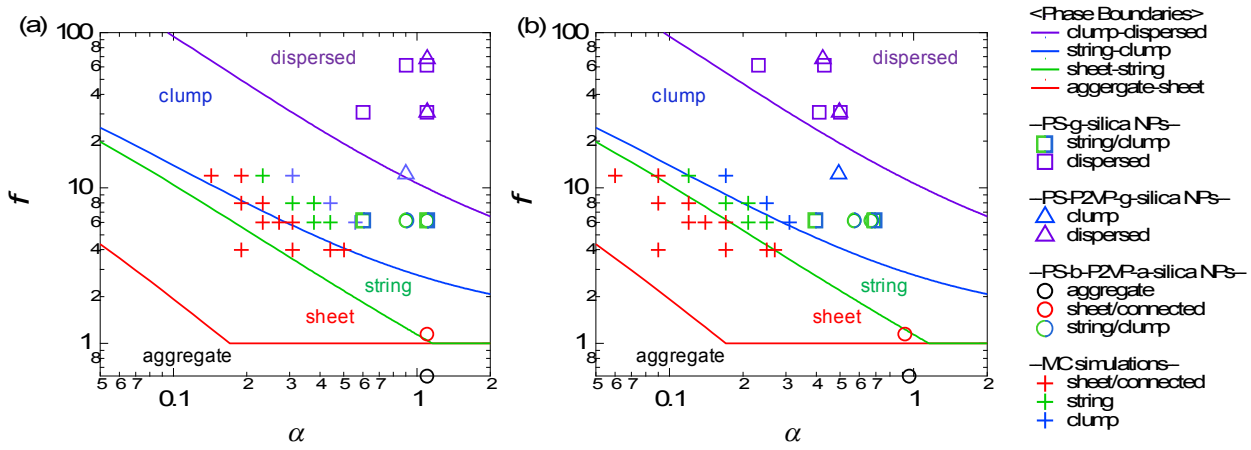

394

395 **Figure 2: Phase diagram of self-assembled structures of PGNPs.** **(a)** plots based on ES model. **(b)**

396 plots based on mES model. f is the number of chains grafted to a NP, and α is defined in the text.

397

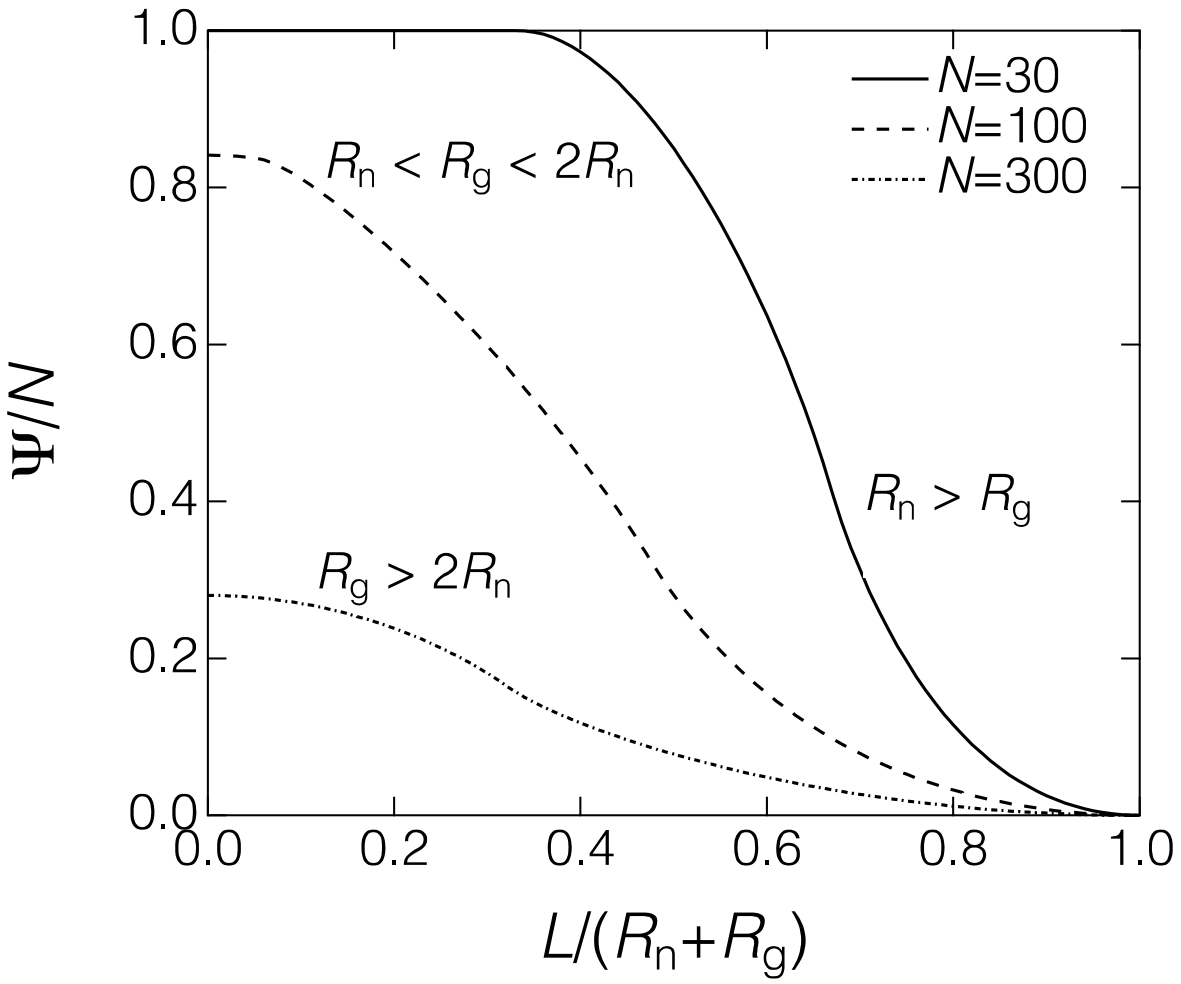

398

399 **Figure 3: Examples of Ψ.** $R_n = 7.0$. $R_g = 3.5, 7.8$ and 15.0 for $N = 30, 100$ and 300.

400

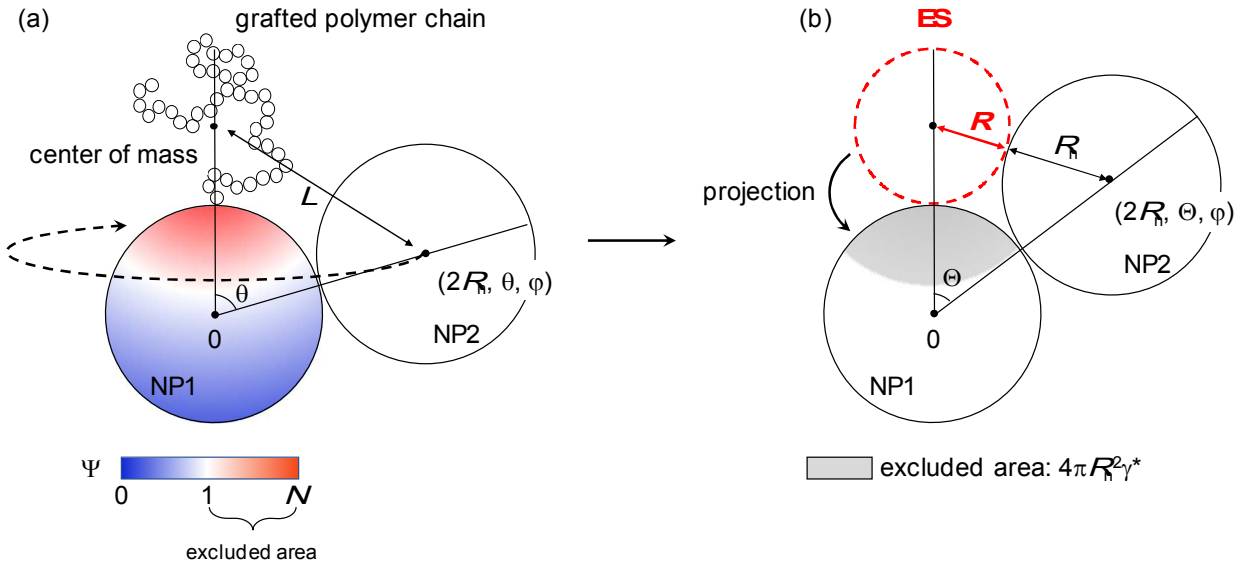

401

402 **Figure 4: Determination of the effective sphere diameter in the mES models. (a)** Searching around a
403 grafted polymer to determine the distribution of Ψ. In the mES model we define the area where $\Psi \geq 1$ as
404 the excluded area, and the ratio of the total excluded area to the NP surface area is γ^*. **(b)** Determining
405 the ES corresponding to γ^*. Grey area indicates the excluded area, $4\pi R_n^2 \gamma^*$ where NP2 cannot contact
406 NP1 in. The dashed line represents the corresponding ES whose size is determined using Eq. (1):
407 $R = 2\gamma^* R_n/(1 - 2\gamma^*)$. Θ is the contact angle between NP1, NP2 and ES, and it follows from $\cos\Theta =$
408 $R_n(R_n + R_g)^{-1}$.

409

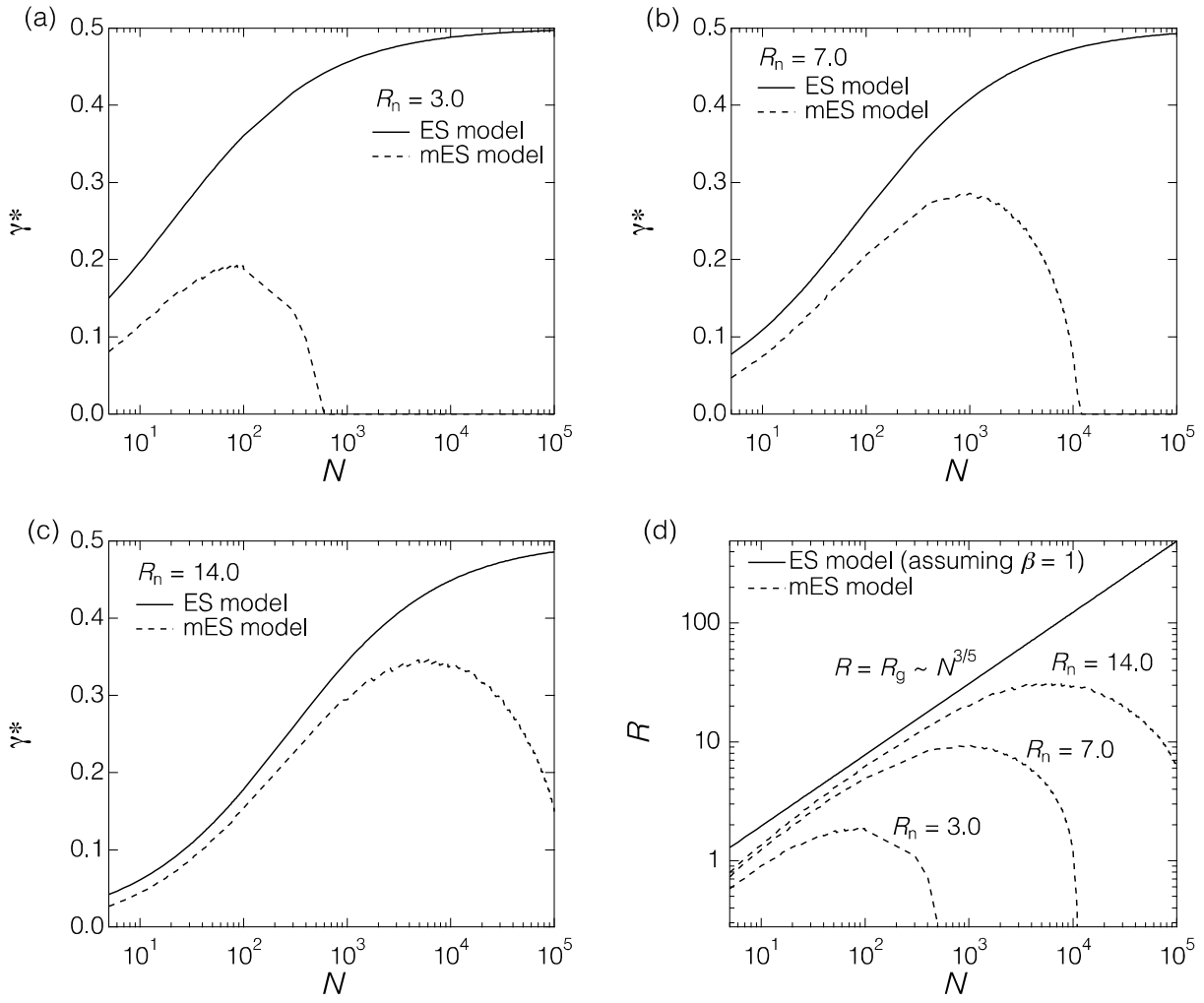

Figure 5: Comparison of mES model with ES model. Comparison of γ^*: **(a)** $R_n = 3.0$. **(b)** $R_n = 7.0$. **(c)** $R_n = 14.0$. **(d)** Comparison of R derived from γ^* and Eq. (1).

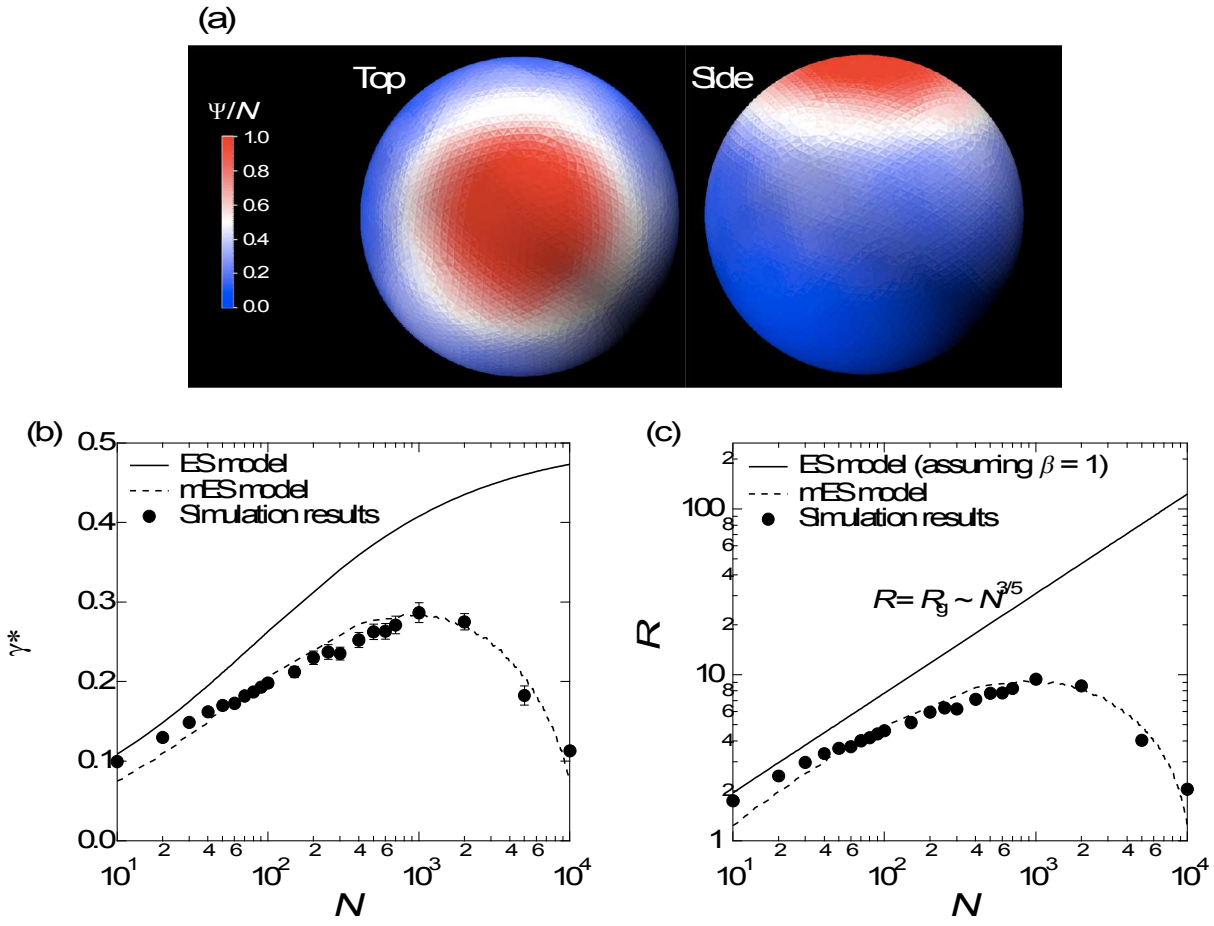

414

415 **Figure 6: Excluded area of single grafted chain on NP1 surface to a second NP (NP2). (a)** An

416 example of the surface distribution of $\langle p_i \rangle_t$. We set the following parameters: $R_n = 7.0$, $N = 200$, $f = 1$,

417 $R_g = 11.3$. We measured $\gamma^* = 0.23$. Color indicates value of $\langle p_i \rangle_t$. **(b)** N-dependence of γ^*. **(c)** N-

418 dependence of R derived using the γ^* and Eq. (1). Error bars show standard error.

419

420

c

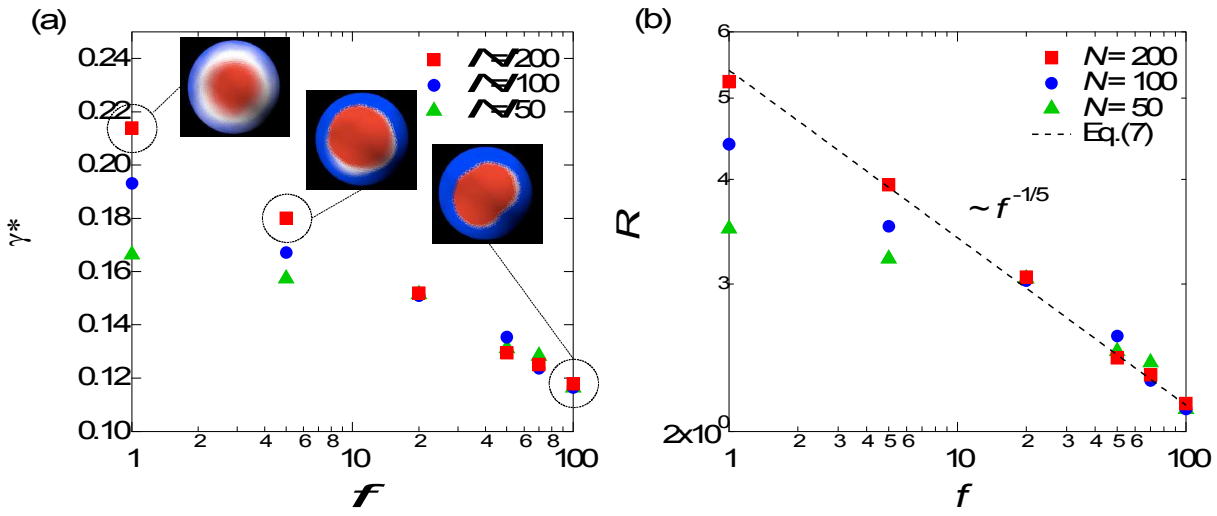

421

422 **Figure 7: Effect of adding grafted polymer chains on the NP1 surface on γ^* and R. (a)** f-dependence

423 of γ^*. Note that γ^* represents the fraction of the NP1 surface that is excluded to NP2 due to presence of a

424 single grafted chain. Pictures shows the surface distribution of $\langle p_i \rangle_t$ for $N = 200$ and $R_n = 7.0$. The

425 color scheme is the same as in Figure 6(a) **(b)** f-dependence of R. The dashed lines represent Eq. (7).

426

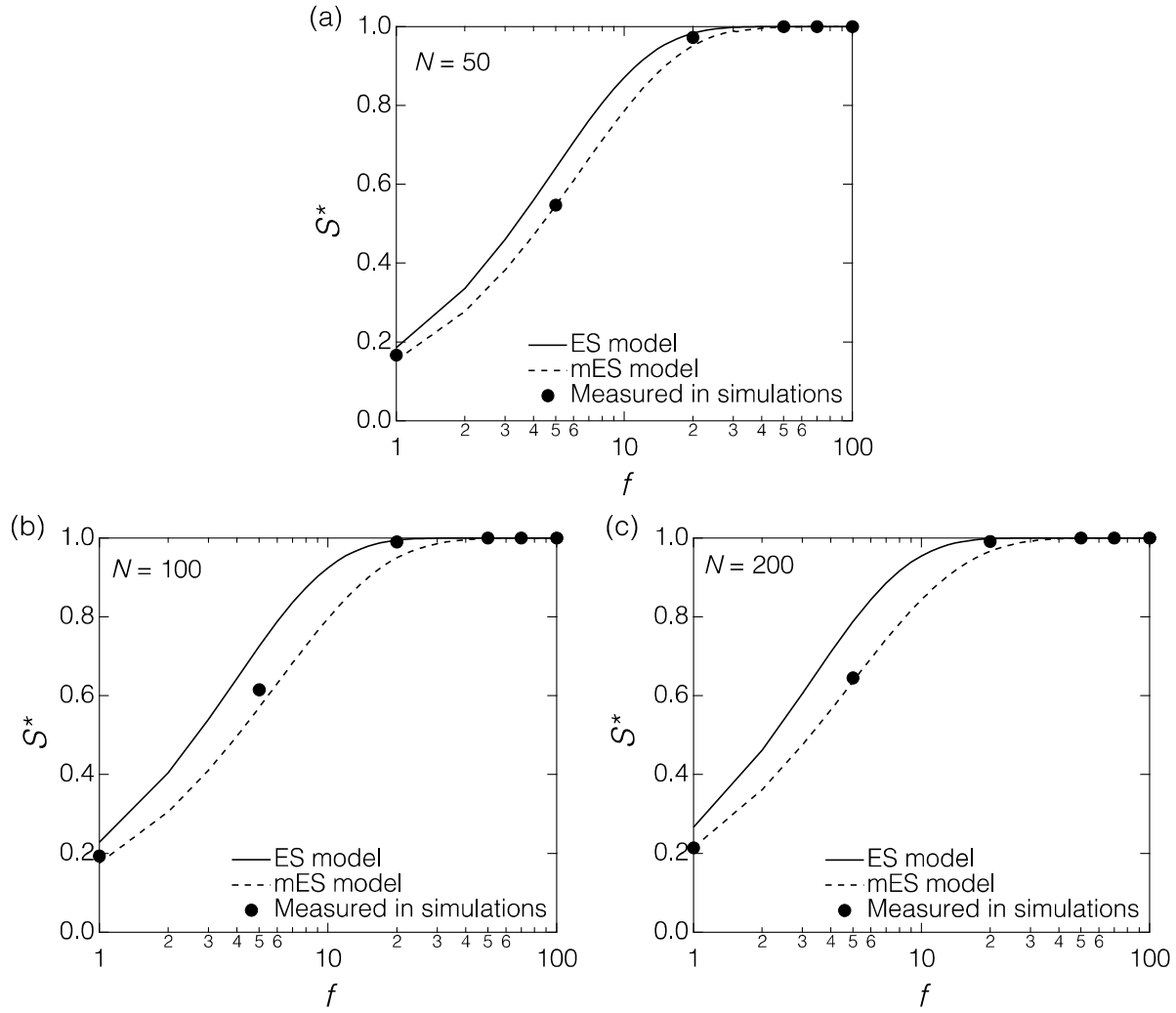

427

428 **Figure 8: f-dependence of S^*.** $R_n = 7.0$. **(a)** $N = 50$. **(b)** $N = 100$. **(c)** $N = 200$.

429

430 **Table 1(a) Experimental conditions and parameters.** R, γ^* and $S^*$are calculated by the mES model.

431 *These parameters were obtained from references.

System	R_n (nm)	N	f	Morphology	R_g (nm)	R(nm)	γ^*	S^*	α
I) PS-g-silica NPs Ref. [10]	7.0	489.68	6.16	string/clump	4.52	2.78	0.14	0.58	0.40
	7.0	1517.04	6.16	string/clump	7.95	4.80	0.20	0.71	0.69
	7.0	1538.46	30.80	dispersed	8.01	3.51	0.17	0.99	0.50
	7.0	1017.76	30.80	dispersed	6.51	2.87	0.15	0.99	0.41
	7.0	432.07	61.60	dispersed	4.24	1.62	0.09	1.00	0.23
	7.0	1480.77	61.60	dispersed	7.85	3.02	0.15	1.00	0.43
II) PS-P2VP-g-silica NPs Ref. [32]	7.0	998.56	12.32	clump	6.45	3.45	0.17	0.87	0.49
	7.0	1507.44	30.79	dispersed	7.93	3.49	0.17	0.99	0.50
	7.0	1488.24	67.73	dispersed	7.87	2.97	0.15	1.00	0.42
III) PS-b-P2VP-a-silica NPs Ref. [33]	7.0	1425.83	0.62	aggregate	7.71	6.75	0.25	0.11	0.96
	7.0	1425.83	1.23	sheet	7.71	6.75	0.24	0.27	0.92
	7.0	1425.83	6.16	string/clump	7.71	6.75	0.20	0.86	0.67
	7.0	1056.17	6.16	string/clump	6.63	5.70	0.18	0.81	0.57

*

Table 1(b) Simulation conditions and parameters. R, γ^* and S^* are calculated by the mES model.

*These parameters were obtained from references.

System	R_h (σ)	N	f	Morphology	R_g (σ)	R(σ)	γ^*	S^*	α
IV) MC simulations Ref. [10]	3.75	0	0	aggregates	0	0	0	0	0
	3.75	3	4	sheet	0.71	0.34	0.04	0.15	0.09
	3.75	6	4	sheet	1.16	0.63	0.07	0.25	0.17
	3.75	10	4	sheet	1.65	0.92	0.10	0.33	0.25
	3.75	12	4	sheet	1.88	1.03	0.11	0.35	0.27
	3.75	4	6	sheet	0.87	0.45	0.05	0.27	0.12
	3.75	5	6	sheet	1.02	0.53	0.06	0.31	0.14
	3.75	6	6	sheet	1.16	0.63	0.07	0.35	0.17
	3.75	8	3	sheet	0.71	0.34	0.04	0.28	0.09
	3.75	8	4	sheet	0.87	0.45	0.04	0.35	0.12
	3.75	2	12	sheet	0.54	0.23	0.03	0.29	0.06
	3.75	3	12	sheet	0.71	0.34	0.04	0.39	0.09
	3.75	6	8	string	1.41	0.78	0.09	0.40	0.21
	3.75	8	6	string	1.16	0.63	0.07	0.44	0.17
	3.75	6	10	string	1.65	0.92	0.10	0.45	0.25
	3.75	8	8	string	1.41	0.78	0.09	0.50	0.21
	3.75	12	4	string	0.87	0.45	0.05	0.47	0.12
	3.75	14	6	clump	2.09	1.17	0.12	0.51	0.31
	3.75	10	8	clump	1.65	0.92	0.10	0.55	0.25
	3.75	6	12	clump	1.16	0.63	0.07	0.58	0.17

435

436

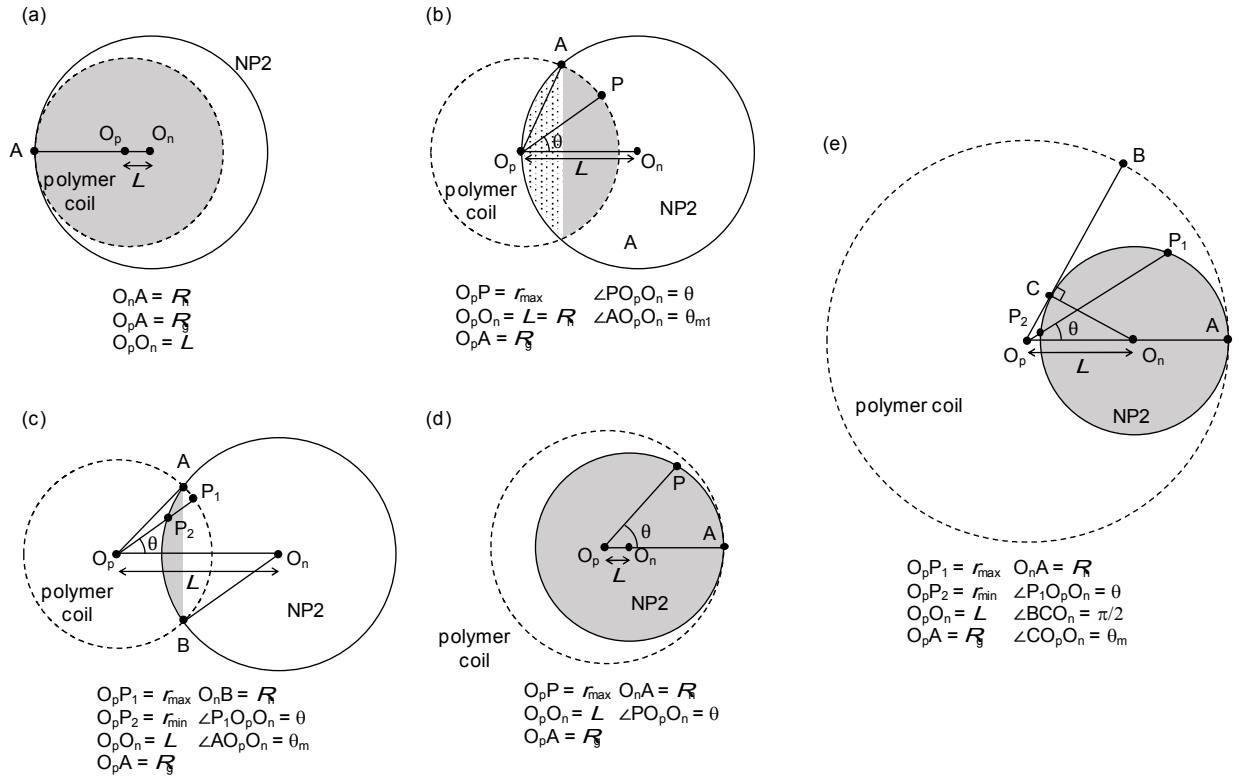

Figure A1: Schematic of geometric relation between the grafted polymer coil and the NP2. The dashed and solid lines represent a grafted polymer coil (radius of R_g) and a NP2 (radius of R_n). NP1 which the polymer coil is grafted on is not shown.

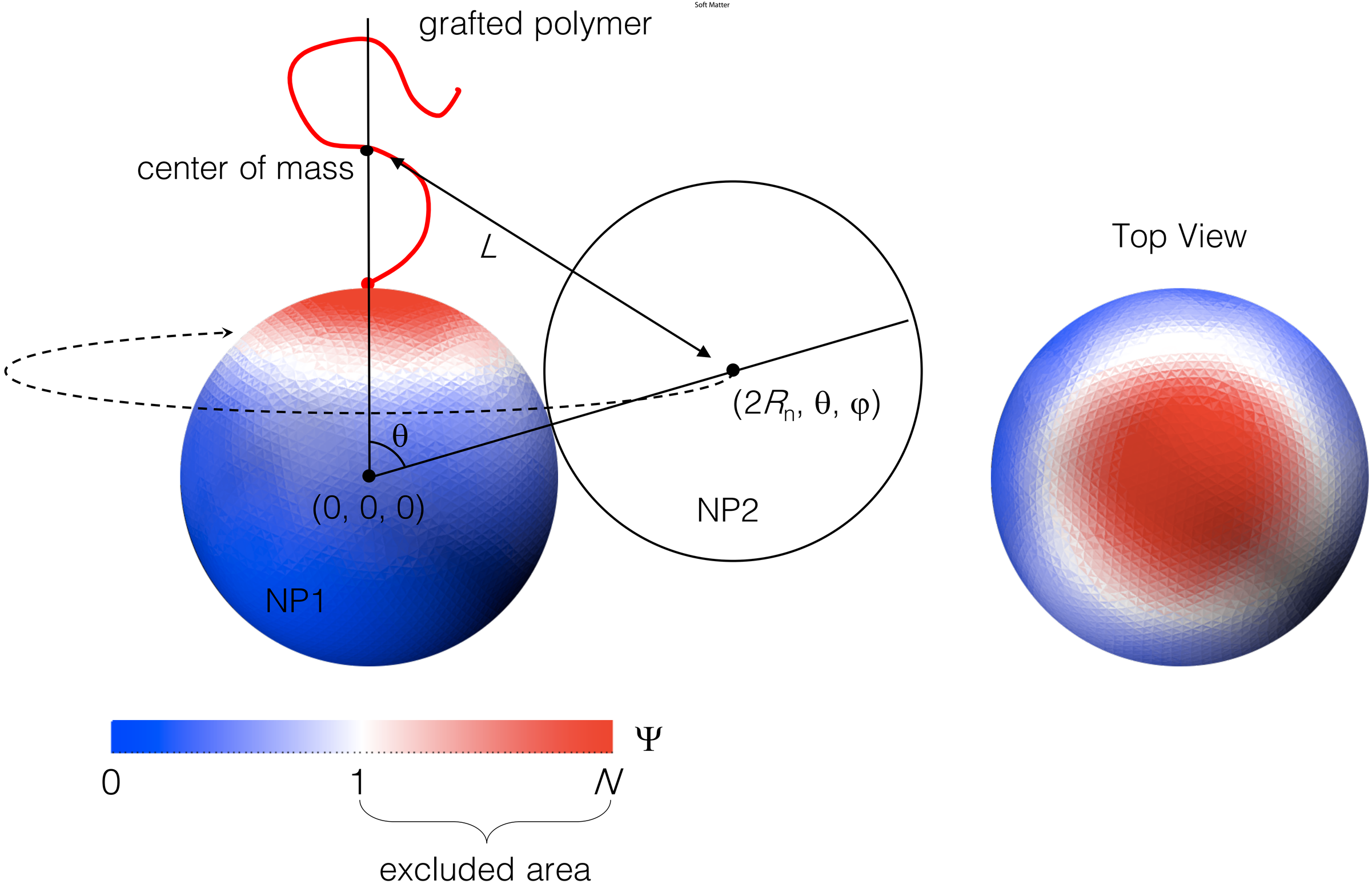
grafted polymer
center of mass
L
θ
(0, 0, 0)
NP1
(2R_n, θ, φ)
NP2
Top View
Ψ
0
1
N
excluded area